Self-assembly as a design tool for the integration of photonic structures into excitonic solar cells

S. Guldin[a], P. Docampo[b], S. Hüttner[a], P.Kohn[a], M. Stefik[c], H.J. Snaith[b], U. Wiesner[c] and U. Steiner[a]

[a]Department of Physics, University of Cambridge, JJ Thomson Ave, Cambridge CB30HE, UK;
[b]Physics Department, University of Oxford, Parks Road, Oxford, OX13PU, UK;
[c]Department of Materials Science & Engineering, Cornell University, Ithaca, NY 14853, USA

ABSTRACT

One way to successfully enhance light harvesting of excitonic solar cells is the integration of optical elements that increase the photon path length in the light absorbing layer. Device architectures which incorporate structural order in form of one- or three-dimensional refractive index lattices can lead to the localization of light in specific parts of the spectrum, while retaining the cell's transparency in others. Herein, we present two routes for the integration of photonic crystals (PCs) into dye-sensitized solar cells (DSCs). In both cases, the self-assembly of soft matter plays a key role in the fabrication process of the TiO_2 electrode. One approach relies on a combination of colloidal self-assembly and the self-assembly of block copolymers, resulting in a double layer dye-sensitized solar cell with increased light absorption from the 3D PC element. An alternative route is based on the fact that the refractive index of the mesoporous layer can be finely tuned by the interplay between block copolymer self-assembly and hydrolytic TiO_2 sol-gel chemistry. Alternating deposition of high and low refractive index layers enables the integration of a 1D PC into a DSC.

Keywords: Dye-sensitized solar cell, photonic crystal, photovoltaics, self-assembly, polymer, TiO_2

1. INTRODUCTION

Light harvesting in excitonic solar cells is fundamentally related to the absorption spectrum of the light-sensitive component. In the case of the conventional DSC,[1] sensitization is realized by the chemisorption of a monolayer of dye molecules onto a nanoporous TiO_2 network. Upon excitation of the dye, electrons are injected into the TiO_2 , while the oxidized dye is regenerated by the surrounding iodine-based electrolyte*. Overall conversion efficiencies above 11% have been reported.[3] In the light of its cost-efficient and non-toxic components, this photovoltaic platform has attracted wide interest in research and industry. One way to further improve the efficiency of the device is to broaden region of maximum photon-to-electron conversion efficiency (EQE). The EQE can reach values around 90% in the region of high extinction of the dye, typically in a spectral range from $510-560\,\mathrm{nm}$. In contrast, the EQE drops significantly in the tail of the absorption spectra of the dye.[4] The development towards dyes with a panchromatic absorption spectrum is of central importance in this respect.[5] A complimentary route to reach broader absorption is the integration of optical elements in the device architecture. These can increase the optical path of the light and thereby the probability of the photons to be absorbed. The introduction of scattering elements in form of titania particles of several hundred nanometers in size has been theoretically described as particularly beneficial[6,7] and is now a common element in record efficiency cells.[3,8] Over the years a variety of concepts have been developed, where the scattering particles are positioned either within or on top of the working electrode.[4,9] Recently much progress has been made in the fabrication of mesoporous scattering particles of controlled size which can also contribute to light absorption and electron generation due to their

Further author information:
S.G.: E-mail: sg506@cam.ac.uk, Telephone: +44 1223 337285
U.S.: E-mail: u.steiner@phy.cam.ac.uk , Telephone: +44-1223-337390

*There is now a wide range of different DSC platforms, which differ in the type of metal oxide network, sensitizer and regenerating hole transporting material. Please see ref[2] for an extensive review.

Next Generation (Nano) Photonic and Cell Technologies for Solar Energy Conversion II, edited by Loucas Tsakalakos,
Proc. of SPIE Vol. 8111, 811108 · © 2011 SPIE · CCC code: 0277-786X/11/$18 · doi: 10.1117/12.893798

largely increased surface area.[10–12] While the implementation of scattering particles has proven highly beneficial for enhanced light absorption, the diffusive scattering over a broad spectral range has the detrimental effect of turning the cells opaque. This deprives the DSC from one of its unique selling points and thus, its potential for integrated architecture. As an alternative, photonic crystal (PC) elements have been proposed with the aim to enhance light harvesting in specific parts of the spectrum while preserving the cell's transparency in others. The early experimental work of Halaoui, Mallouk and coworkers[13,14] on 3D PCs realized by TiO_2 inverse opal structures has inspired a whole field of experimental and theoretical research. The physical origin for the experimentally observed positive effect of 3D PCs on light absorption in the device was initially unclear. The localization of heavy photons near the edges of a photonic bandgap,[15] Bragg diffraction in the periodic lattice[16] and multiple scattering at disordered regions of the PC[17] were discussed to be likely candidates. Mihi and Míguez later introduced a model, which promised the formation of multiple resonant modes and therefore significant absorption enhancement throughout the photonic bandgap of the PC.[18] According to this model, resonant cavities are determined by the penetration depth of the incoming light into the PC and the thickness of the mesoporous film between the PC and the substrate. These cavities give rise to the localization of photons in the device, thus an enhanced absorption probability. A double layer configuration, with a mesoporous TiO_2 layer being sandwiched between the transparent conducting substrate and the 3D PC was therefore promised most efficient but the experimental realization proved difficult.[19,20] As a vital alternative, Míguez and coworkers proposed the integration of a 1D PC into the device architecture which was easier to fabricate and less susceptible to defects.[21] In this case, the refractive index lattice is realized by the sequential deposition of high and low refractive index layers, typically nanoparticle-based mesoporous films of TiO_2 and SiO_2.[22] The effect of the 1D PC on the light harvesting of the DSC has been experimentally and theoretically investigated and current results are highly promising.[21,23] However, the use of SiO_2 in the current configuration as the low refractive building block has one major drawback: the 1D PC stack is non-conducting, and can therefore not contribute to light absorption and conversion in the overall device.

Here, we present our recent developments to the field of PC based DSCs. The self-assembly of soft matter plays a key role in our routes to integrated TiO_2 electrode architectures. One approach relies on a combination of colloidal self-assembly and the self-assembly of block copolymers, resulting in a double layer dye-sensitized solar cell with increased light absorption from the 3D PC element. An alternative route is based on the fact that the porosity and therefore refractive index of the mesoporous layer can be finely tuned by the interplay between block copolymer self-assembly and hydrolytic TiO_2 sol-gel chemistry. Alternating deposition of high and low porosity TiO_2 layers enables the stacking of a dielectric lattice and therefore the assembly of a conducting 1D PC into a DSC.

2. EXPERIMENTAL

2.1 Fabrication of double layer electrode integrating a 3D PC

For the fabrication of the block-copolymer assembled mesoporous underlayer, a titanium containing sol was prepared by the rapid addition of 0.69 ml HCl (37%) to 1 ml titanium ethoxide (purum) under vigorous stirring. A solution of 0.1 g poly(isoprene-*block*-ethleneoxide) copolymer (PI-*b*-PEO) ($M_n = 35.7$ g/mol, 23 wt% PEO) in 7 ml of tetrahyfrofuran (THF) was prepared alongside. After 1.5 hours of stirring, 0.873 ml of the resulting sol was added to the polymer solution, before the volatile components were evaporated at 50° C in a Petri dish. Shortly after, the dry material was redissolved in an azeotrope mixture of of 73 vol% toluene and 27 vol% 1-butanol. Films were then deposited by spin-coating of the 20w% solution (5 s, 1500 rpm). After annealing of the films (slow ramping up to 130° C), a thin overlayer was removed by reactive ion etching of CF_4. The 3D PC was then fabricated on top of this layer in three steps: a face-centered-cubic colloidal array was deposited by evaporation induced self-assembly of polystyrene spheres. The template was then infiltrated by a binary atmospheric pressure chemical vapor deposition (APCVD). Subsequently, the samples were exposed by another cycle of reactive ion etching. Finally, the TiO_2 double layer structure was revealed by the calcination of the samples at 500 °C. For device characterization, DSCs were assembled following a protocol as described elsewhere (dye N719).[24] Please see ref[25] for further experimental details.

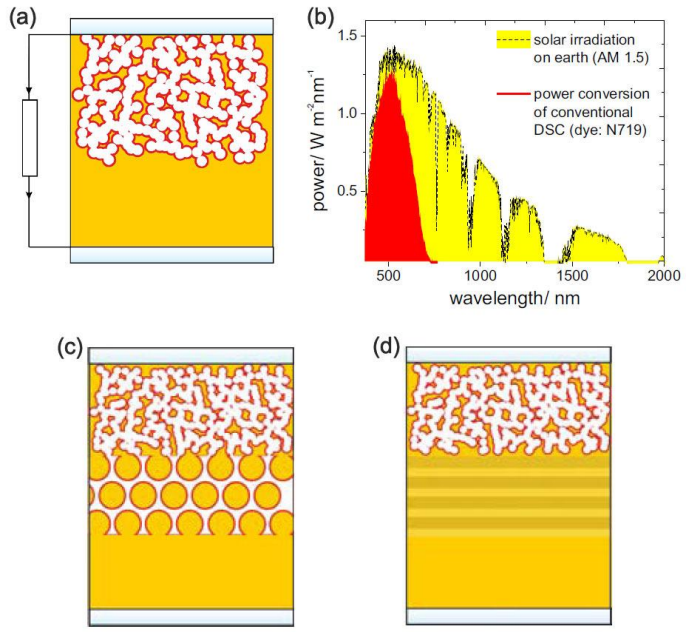

Figure 1. DSC device architectures. (a) Conventional architecture of a DSC. Nm-sized TiO_2 particles form a random electron conducting network of high surface area. A monolayer of light-absorbing dye molecules is chemisorbed onto the TiO_2 and surrounded by a hole-transporting electrolyte. Upon photoexcitation of the dye, electrons are injected into the TiO_2 , while the oxidized dye is regenerated by the electrolyte, which shuttles holes to the counter electrode to complete the circuit. (b) Power spectrum of solar irradiation on earth (AM1.5) and spectrally resolved light-to-electrical energy conversion of a nanoparticle-based DSC sensitized with the dye N719 (EQE results from ref[4]). While state-of-the-art DSCs can almost achieve maximum quantum efficiency in the spectral range around $510 - 560$ nm, light harvesting in the red and near-infrared (at the tail of the absorption spectra) is still relatively low. Device architectures to localize photons of a specific spectral range while retaining the overall transparency of the device include the integration of 3D and 1D photonic crystals (PCs). 3D PCs are typically realized by a TiO_2 inverse opal structure (c). 1D PCs are generally mesoporous Bragg reflectors made of two alternating mesoporous layers of high and low refractive index (d).

2.2 Fabrication of multilayer electrode integrating a 1D PC

Two stock solution with differing ratio of TiO_2 sol to PI-*b*-PEO copolymer were prepared as follows. First the sol was made following a similar procedure as above. TiO_2 to polymer weight ratios of 3:1 and 1:2 were chosen for the high and low refractive index layers, which will be referred to as "$T_{3:1}$" and "$T_{1:2}$", respectively. For $T_{3:1}$, 0.1 g of PI-*b*-PEO (molecular weight $M_n = 34.4\,\mathrm{kg\ mol^{-1}}$, 28 wt% PEO) was dissolved in 7 ml THF before 1.31 ml sol was subsequently added. After the evaporation of volatile components (see above) the hybrid material was redissolved in a solvent mixture of 49 vol% toluene and 51 vol% 1-butanol. For the preparation of the $T_{1:2}$ stock solution, 0.22 ml sol was added to the polymer solution (0.1 g PI-*b*-PEO in 7 ml THF) and dried. This material was redissolved in an azeotrope mixture of toluene and 1-butanol. The concentrations of the stock solutions were adjusted to meet the film thickness requirements previously calculated. Film deposition was carried out by spin-coating of the solutions at 2000 rpm onto pre-cleaned glass. After each deposition an annealing cycle of 10 min at 100 °C, 200 °C and 300 °C was applied. Layers from $T_{3:1}$ and $T_{1:2}$ were deposited in alternating fashion, each followed by an annealing cycle to build-up the stack. Finally the stack was calcined at 500 °C (3 hours, heat ramp 5 °C $\mathrm{min^{-1}}$) to remove the organic components and crystallize the TiO_2 .

3. RESULTS AND DISCUSSION

Figure 1a and 1b shall illustrate the motivation for the implementation of PC into DSCs. Conventional DSC typically lack conversion efficiency in the tail of the absorption spectrum of the dye, i.e. where the dye itself is poorly absorbing. High efficiency DSCs have therefore scattering elements integrated into their device architecture to increase the optical path lengths and therefore absorption probability. Figure 1c and 1d illustrate two examples for optical components which do not rely on the random diffuse scattering of light, but on the

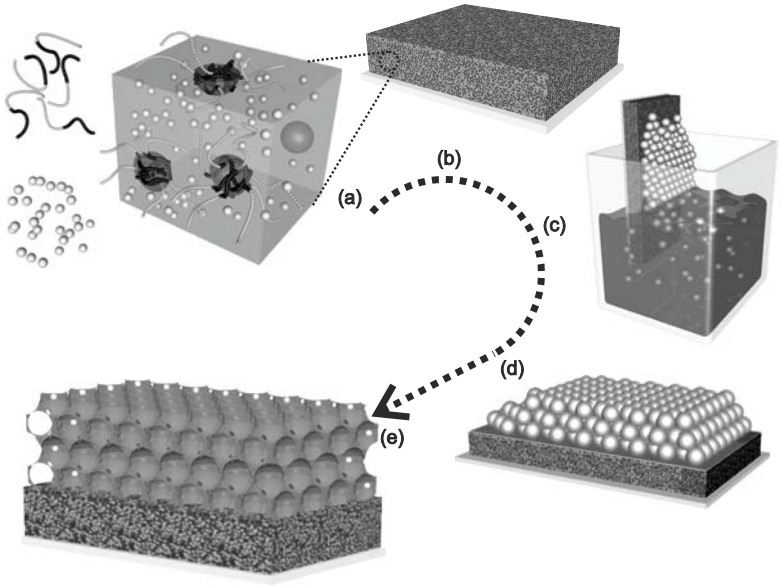

Figure 2. Illustration of the assembly of a double layer electrode. (a) A solution containing PI-b-PEO block copolymer and TiO_2 sol is deposited onto a transparent conducting substrate by spin coating, doctor blading or dip coating. (b) The film is annealed up to 130 °C and placed vertically into a suspension of polystyrene microspheres. Upon evaporation of the solvent an f.c.c. colloidal array is formed by evaporation induced self-assembly. (d) The template is then infiltrated by APCVD of amorphous TiO_2 into the interstitial pores. (e) Finally the samples is calcined to crystallize the TiO_2 double layer structure and remove the organic material. See ref[25] for further details.

localization of photons in the structure. According to Mihi and Míguez, non-absorbed light of energies within the photonic band-gap of the PC, partially penetrates into the 3D PC as an evanescent wave. Resonant cavities are formed, determined by the distance of the penetration depth and the thickness of the mesoporous film. These lead to multiple resonant modes and therefore enhanced absorption probability over a wide spectral range.[18] The integration of a 1D PC in a multilayer structure can have a similar effect by increasing the electromagnetic field in the absorbing layer. While theoretical calculations prove both structures as highly promising,[18,23] state-of-the-art fabrication routes can not yet take full advantage of the concept.

3.1 Integration of a 3D PC into a DSC

Figure 2 illustrates our fabrication route for a fully self-assembled double layer structure, coupling an inverse opal TiO_2 PC to a mesoporous underlayer. The main challenge in previous approaches was to grow an inverse opal 3D PC layer on top of a mesoporous underlayer. The filling of the colloidal template by vapor phase deposition would typically equally infiltrate the underlying nanoparticle-based mesoporous film. This leads to clogging of the nanopores which inhibits sensitization and electrolyte propagation within the double layer device. The alternative configuration of depositing a mesoporous layer on top of the PC[13,14] was found detrimental for two reasons - the device had to be illuminated from the backside and the proposed resonant modes could not be exploited.[18] One way to circumvent this problem is the infiltration of the mesoporous network with a protecting material prior to the deposition of the 3D PC. This route was introduced by Mallouk and coworkers but the connectivity between both layers was identified to be not good enough to take full advantage of the concept.[20] Figure 2 illustrates our approach to this challenge. In our route, the mesoporous underlayer is fabricated by the co-assembly of block copolymers and TiO_2 sol. Before calcination, the hybrid layer is non-porous, leaving the mesopores unaffected by the fabrication of a 3D PC top layer. Only in a final calcination step the organic material is then removed to reveal the double layer TiO_2 photoanode.

The resulting morphology of the double layer structure following this fabrication route is shown in Figure 3. The deposition and the filing of the colloidal template has been successful, as discernible in Figure 3a. Figure 3b shows the long range order of the TiO_2 inverse opal structure. The crucial interface between both layers is

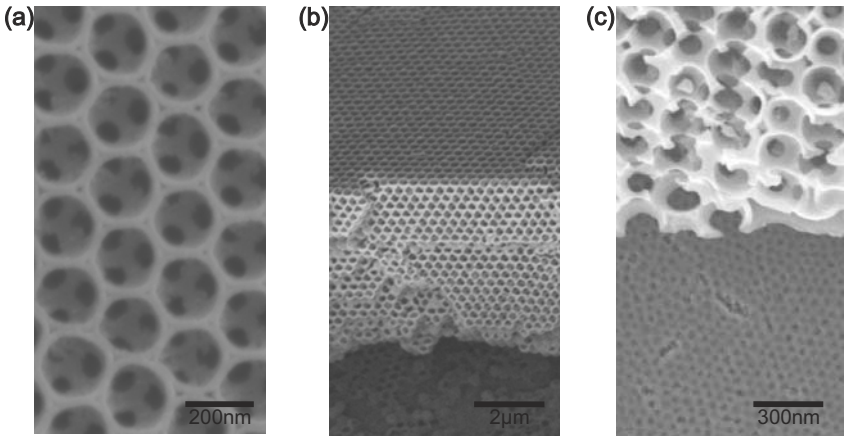

Figure 3. Scanning electron micrographs of the TiO_2 double layer structure. (a) Top view of the (111) plane of the TiO_2 inverse opal. (b) Cross-sectional view of the TiO_2 double layer structure, with the inverse opal PC on top of a mesoporous layer. (c) Close-up view of the double layer interface, showing complete connectivity between the mesopores and the micropores.

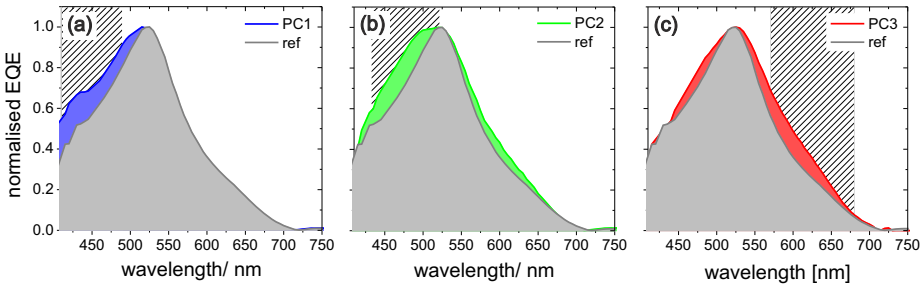

Figure 4. Normalized photon-to-electron conversion efficiency (EQE) of double layer arrays compared to reference cell with only a single, mesoporous layer of similar surface area to the double layer devices PC1 and PC3. The patterned area illustrates the spectral region where the 3D PC is active in the assembled device. Different dielectric lattices were realized by adjusting the size of the PS spheres in the fabrication process. (a) PC1 has a final pore size of 160 nm. (b) PC2 shows 180 nm pores and exhibits an inverse opal film thickness which is doubled compared to PC1 and PC3. (c) PC3 exhibits a pore size of 240 nm as measured by electron microscopy and verified by the position of the Bragg peak.

shown in Figure 3c. Good pore connectivity between the micropores of the 3D PC and the mesopores of the underlying layer is seen, promising full sensitization of the structure, unhindered electrolyte propagation and good electronic connectivity.

The effect of the PC top layer on the absorption spectrum of the overall device was herein of particular interest. Double layer devices incorporating 3D PCs of different pore diameter (related to varied sphere sizes in the fabrication) were compared to the absorption of a reference cell without a PC but a thicker mesoporous layer to ensure similar overall surface area. Alongside, PC layers were optically characterized. The spectral region of the stop-band in the device environment is illustrated at patterned region in the graphs in Figure 4. From comparing the normalized photon-to-electron conversion efficiency (EQE) of different PC double layer devices with the reference cell, it is evident that the observed absorption spectrum of the device is strongly influenced by the functioning of the PC top layer. With the position of the Bragg peak moving from the deep blue to the red of the spectrum, the broadening of the normalized absorption peak moves alongside. The physical origin of this effect cannot be solely related to scattering effects. These would occur most efficiently around $\lambda \approx 1.33 \cdot d$, where d is the diameter of the scattering object,[6] so in the deep blue for all 3 model systems. Furthermore, scattering at defect planes should be closely related to the ratio of $d_{\mathrm{opal}}/\lambda$, which leads to very low scattering probabilities in the red.[17] Nevertheless a small fraction of the observed absorption shift can be correlated to scattering, best seen

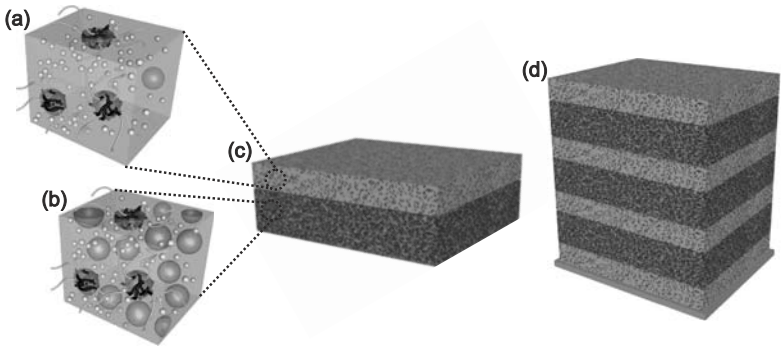

Figure 5. Schematic of the fabrication route for the anatase 1D PC. Two stock solutions are prepared with a TiO_2 to polymer weight ratio of (a) 3:1 ($T_{3:1}$) and (b) 1:2 ($T_{1:2}$), respectively. The differing weight ratio of organic and inorganic material is reflected in the micro-phase separation of the co-assembled material. A higher TiO_2 content results in a denser structure with less pores and therefore higher refractive index. Increasing the organic content leads to a more porous network of lower refractive index. MDBR stacks are built-up by the spin coating of alternating solutions, followed by a 30 min annealing protocol after each deposition cycle (c, d). The final stack is the calcined at 500°C to crystallize the TiO_2 network and remove the organic material. See ref[26] for further details.

in Figure 4c as a slightly increased absorption shoulder in the blue. Furthermore, the slight increase in relative absorption between 550 nm and 650 nm in PC2 can be related to the increased overall surface area of the device, compared to PC1, PC3 and the reference cell. Due to the poor absorption of the dye in this wavelength range, an increased film thickness will lead to a relative enhancement of the EQE in this region. For the interested reader we refer to ref[25] for a full discussion of the absorption features. In conclusion, the presented route leads to a TiO_2 electrode architecture which couples a high surface area mesoporous underlayer to an optically and electrically active 3D PC top layer. In contrast to earlier approaches the structure exhibits fully interconnected top and bottom layers with a smooth interface. As a result, we could observe that the absorption of the device is strongly affected by the action spectrum of the 3D PC.

3.2 Integration of a 1D PC into a DSC

As an alternative concept to the integration of 3D PC into DSCs, Míguez and coworkers recently proposed the integration of a 1D PC.[21] The 1D refractive index lattice is realized by the alternating deposition of high and low refractive index mesoporous layers, typically nanoparticle-based films of TiO_2 and SiO_2.[22] While theoretical and experimental investigations are highly promising,[21,23] the currently used PC stacks are non-conducting and can therefore not contribute to light absorption and conversion in the overall device.

The fabrication route of a block copolymer based porous 1D PC is illustrated in Figure 5. The refractive index of the resulting mesoporous layer is a function of the weight ratio between organic and inorganic material during the self-assembly process. Using two differing weight ratios for the film deposition in alternating fashion (in our case 3:1 ($T_{3:1}$) and 1:2 ($T_{1:2}$)), we could build up a stack which is based on a lattice of high and low refractive index layers. The gradual annealing of the stack after each deposition cycle plays a decisive role for the success of this material route. The large volume contraction during the several processing steps from the deposition of the initial hybrid film to the final mesoporous inorganic layer needs to be accommodated to prevent cracking and delamination. We have investigated the time- and temperature dependence of the shrinkage kinetics in detail which enabled us to establish a 30 min temperature annealing protocol. Following this protocol after every layer deposition, we were able to release most volume reduction step-by-step, leading to a crack-free stacking of a multilayer film. Please see ref[26] for details. After the gradual deposition and annealing of each building block, we finally calcine the stack at 500°C, to crystallize the TiO_2 and remove the organics.

The functioning of the 1D PC is illustrated in detail in Figure 6. The alternating electron density of the high and low refractive index mesoporous TiO_2 layers is easily discernible in the cross-sectional transmission electron micrograph shown in Figure 6a. Incoming light is partially reflected at each of the interfaces, leading to multiple interference and therefore a characteristic color appearance. This is exemplarily shown in Figure 6b-e, where

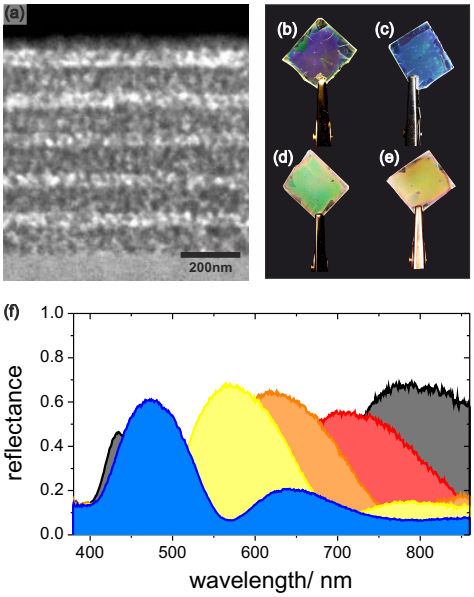

Figure 6. Functioning of the anatase 1D PC. (a) TEM cross-sectional view of a 11 layer stack. Darker layers correspond to the high TiO_2 content in the $T_{3:1}$ layers. Brighter layers are related to the lower electron density in the $T_{1:2}$ layers. Due to the multiple interference of light reflected at the interfaces of the 1D PC, strong structural coloration arises, which is a function of the refractive index and the layer thickness of the building blocks. (b)-(e) Photographs illustrating the reflection characteristics of 1D PCs, consisting of 5 $T_{3:1}$ and 4 $T_{1:2}$ layers. The variation of the layer thickness of $T_{1:2}$, leads to characteristic reflection in (b) violet, (c) blue, (d) green, and (e) yellow, respectively. (f) Experimental reflectance of different stacks, where the five layers of $T_{3:1}$ were kept constant at $d_{3:1} \approx 75$ nm and the four layers of $T_{1:2}$ $d_{1:2}$ were varied between ≈ 78 nm and ≈ 202 nm

the refractive index of the building blocks as well as the thickness of the $T_{3:1}$ layers is kept constant, while the thickness of the $T_{1:2}$ layers is finely tuned. The reflection properties was also characterized spectroscopically, plotted in Figure 6f. The layer thickness of $T_{1:2}$ ($d_{1:2}$) was varied between ≈ 78 nm and ≈ 202 nm, while the five layers of $T_{3:1}$ were kept constant at $d_{3:1} \approx 75$ nm. Direct comparison between the experimentally observed performance and calculations of an ideal 1D PC (with $T_{1:2}$ and $T_{3:1}$ layers being building blocks of an ideal lattice) are very similar and show that the regularity of the stack is close to perfection (please see ref[26] for further details).

Our route to mesoporous TiO_2 films, using the co-assembly of PI-*b*-PEO copolymer and hydrolytic sol has several advantages over the currently widespread nanoparticle approach for the use as light harvesting element in DSCs. The pore size of the network is relatively uniform and can be finely tuned over a wide parameter range, as this is determined by the molecular weight of the polymer's PI block. In earlier work, we could show that the average pore diameter could be tuned between 20 nm and 80 nm by using different block copolymers.[27] This is in stark contrast to nanoparticle networks, where the pore formation is based on the random dense packing of nanoparticles. As a consequence these random networks suffer from polydisperse pore size distribution and lack control over porosity and pore sizes. The block copolymer derived stack is fully conducting as both building blocks are made of TiO_2 , which enables light absorption and charge generation by the 1D PC, integrating the optical element as an active component in the device. Furthermore we have shown that the block copolymer directed TiO_2 networks allow fine control over electron conductivity[28] and distribution of sub-bandgap states[29] which is particular important for solid state DSCs.[30]

4. CONCLUSIONS

In summary we have suggested two material routes for the effective integration of 1D and 3D PCs into dye-sensitized solar cells. Self-assembly material synthesis on two length-scales enabled us realize a sought-after

device architecture, which couples a 3D PC to a mesoporous underlayer. The resulting double layer structure shows electric and pore connectivity at the mesoporous and the microporous level, whichs allows effective dye sensitization, electrolyte infiltration, and charge collection from both the mesoporous and the 3D PC layers. The absorption spectrum of the device is not only a function of the dye but is strongly manipulated by the action spectrum of the 3D PC. Besides, we have developed a materials route for the integration of a 1D PC. Unique features include the fine control of pore size and porosity as well as the fact that the resulting bicontinuous network is highly ordered, fully conductive and of outstanding optical quality. Both concepts open up a wide parameter space for effective light management in DSCs and promise enhanced efficiencies by harvesting PC-induced resonances.

Acknowledgments

This publication is based on work supported in part by Award No. KUS-C1-018-02, made by King Abdullah University of Science and Technology (KAUST), the EPSRC (EP/F056702/1 and EP/F065884/1), the Department of Energy (DE-FG02 87ER45298) through the Cornell Fuel Cell Institute (CFCI) and the National Science Foundation (DMR-0605856).

REFERENCES

[1] O'Regan, B. and Grätzel, M., "A low-cost, high-efficiency solar-cell based on dye-sensitized colloidal tio$_2$ films," *Nature* **353**(6346), 737–740 (1991).

[2] Hagfeldt, A., Boschloo, G., Sun, L., Kloo, L., and Pettersson, H., "Dye-sensitized solar cells," *Chemical Reviews* **110**(11), 6595–6663 (2010).

[3] Chiba, Y., Islam, A., Watanabe, Y., Komiya, R., Koide, N., and Han, L., "Dye-sensitized solar cells with conversion efficiency of 11.1%," *Japanese Journal Of Applied Physics Part 2-Letters & Express Letters* **45**(24-28), L638–L640 (2006).

[4] Wang, Z.-S., Kawauchi, H., Kashima, T., and Arakawa, H., "Significant influence of TiO_2 photoelectrode morphology on the energy conversion efficiency of n719 dye-sensitized solar cell," *Coordination Chemistry Reviews* **248**, 1381–1389 (2004).

[5] Yum, J.-H., Baranoff, E., Wenger, S., Nazeeruddin, M. K., and Grätzel, M., "Panchromatic engineering for dye-sensitized solar cells," *Energy & Environmental Science* **4**(3), 842–857 (2011).

[6] Usami, A., "Theoretical study of application of multiple scattering of light to a dye-sensitized nanocrystalline photoelectrochemical cell," *Chemical Physics Letters* **277**(1-3), 105–108 (1997).

[7] Ferber, J. and Luther, J., "Computer simulations of light scattering and absorption in dye-sensitized solar cells," *Solar Energy Materials And Solar Cells* **54**(1-4), 265–275 (1998).

[8] Nazeeruddin, M. K., Bessho, T., Cevey, L., Ito, S., Klein, C., De Angelis, F., Fantacci, S., Comte, P., Liska, P., Imai, H., and Grätzel, M., "A high molar extinction coefficient charge transfer sensitizer and its application in dye-sensitized solar cell," *Journal Of Photochemistry And Photobiology A-Chemistry* **185**(2-3), 331–337 (2007).

[9] Hore, S., Vetter, C., Kern, R., Smit, H., and Hinsch, A., "Influence of scattering layers on efficiency of dye-sensitized solar cells," *Solar Energy Materials and Solar Cells* **90**(9), 1176–1188 (2006).

[10] Sauvage, F., Chen, D., Comte, P., Huang, F., Heiniger, L.-P., Cheng, Y.-B., Caruso, R. A., and Grätzel, M., "Dye-sensitized solar cells employing a single film of mesoporous TiO_2 beads achieve power conversion efficiencies over 10%.," *ACS Nano* **4**(8), 4420–5 (2010).

[11] Chen, B. D., Huang, F., Cheng, Y.-B., and Caruso, R. A., "Mesoporous anatase TiO_2 beads with high surface areas and controllable pore sizes : a superior candidate for high-performance dye-sensitized solar cells," *Advanced Materials* **21**, 2206–2210 (2009).

[12] Yu, I. G., Kim, Y. J., Kim, H. J., Lee, C., and Lee, W. I., "Size-dependent light-scattering effects of nanoporous TiO_2 spheres in dye-sensitized solar cells," *Journal Of Materials Chemistry* **21**(2), 532–538 (2011).

[13] Nishimura, S., Abrams, N., Lewis, B. A., Halaoui, L. I., Mallouk, T. E., Benkstein, K. D., Lagemaat, J. V. D., and Frank, A. J., "Standing wave enhancement of red absorbance and photocurrent in dye-sensitized titanium dioxide photoelectrodes coupled to photonic crystals," *Journal of the American Chemical Society* **125**(3), 6306–6310 (2003).

[14] Halaoui, L., Abrams, N., and Mallouk, T., "Increasing the conversion efficiency of dye-sensitized tio$_2$ photoelectrochemical cells by coupling to photonic crystals," *Journal Of Physical Chemistry B* **109**(13), 6334–6342 (2005).

[15] Sakoda, K., "Enhanced light amplification due to group-velocity anomaly peculiar to two- and three-dimensional photonic crystals," *Optics Express* **4**(5), 167–176 (1999).

[16] Mittleman, D., Bertone, J., Jiang, P., Hwang, K., and Colvin, V., "Optical properties of planar colloidal crystals: dynamical diffraction and the scalar wave approximation," *Journal Of Chemical Physics* **111**(1), 345–354 (1999).

[17] Rengarajan, R., Mittleman, D., Rich, C., and Colvin, V., "Effect of disorder on the optical properties of colloidal crystals," *Physical Review E* **71**(1, Part 2), 15968–15976 (2005).

[18] Mihi, A. and Míguez, H., "Origin of light-harvesting enhancement in colloidal-photonic-crystal-based dye-sensitized solar cells," *Journal Of Physical Chemistry B* **109**(33), 15968–15976 (2005).

[19] Mihi, A., Calvo, M. E., Anta, J. A., and Míguez, H., "Spectral response of opal-based dye-sensitized solar cells," *Journal Of Physical Chemistry C* **112**(1), 13–17 (2008).

[20] Lee, S.-H. A., Abrams, N. M., Hoertz, P. G., Barber, G. D., Halaoui, L. I., and Mallouk, T. E., "Coupling of titania inverse opals to nanocrystalline titania layers in dye-sensitized solar cells," *Journal Of Physical Chemistry B* **112**(46), 14415–14421 (2008).

[21] Colodrero, S., Mihi, A., Haggman, L., Ocaña, M., Boschloo, G., Hagfeldt, A., and Míguez, H., "Porous one-dimensional photonic crystals improve the power-conversion efficiency of dye-sensitized solar cells," *Advanced Materials* **21**(7), 764770 (2009).

[22] Colodrero, S., Ocaña, M., Gonzalez-Elipe, A. R., and Míguez, H., "Response of nanoparticle-based one-dimensional photonic crystals to ambient vapor pressure," *Langmuir* **24**(21), 9135–9139 (2008).

[23] Colodrero, S., Mihi, A., Anta, J. A., Ocaña, M., and Míguez, H., "Experimental demonstration of the mechanism of light harvesting enhancement in photonic-crystal-based dye-sensitized solar cells," *Journal Of Physical Chemistry C* **113**, 1150–1154 (2009).

[24] Nedelcu, M., Guldin, S., Orilall, M. C., Lee, J., Hüttner, S., Crossland, E. J. W., Warren, S. C., Ducati, C., Laity, P. R., Eder, D., Wiesner, U., Steiner, U., and Snaith, H. J., "Monolithic route to efficient dye-sensitized solar cells employing diblock copolymers for mesoporous TiO_2," *Journal Of Materials Chemistry* **20**(7), 1261–1268 (2010).

[25] Guldin, S., Hüttner, S., Kolle, M., Welland, M. E., Müller-Buschbaum, P., Friend, R. H., Steiner, U., and Tétreault, N., "Dye-sensitized solar cell based on a three-dimensional photonic crystal," *Nano Letters* **10**(7), 2303–2309 (2010).

[26] Guldin, S., Kolle, M., Stefik, M., Langford, R., Eder, D., Wiesner, U., and Steiner, U., "Tunable mesoporous bragg reflectors based on block-copolymer self-assembly," *Advanced Materials* , Doi: 10.1002/adma.201100640 (2011).

[27] Nedelcu, M., Lee, J., Crossland, E. J. W., Warren, S. C., Orilall, M. C., Guldin, S., Hüttner, S., Ducati, C., Eder, D., Wiesner, U., Steiner, U., and Snaith, H. J., "Block copolymer directed synthesis of mesoporous TiO_2 for dye-sensitized solar cells," *Soft Matter* **5**(1), 134–139 (2009).

[28] Guldin, S., Hüttner, S., Tiwana, P., Orilall, M. C., Ülgüt, B., Stefik, M., Docampo, P., Kolle, M., Divitini, G., Ducati, C., Redfern, S. A. T., Snaith, H. J., Wiesner, U., Eder, D., and Steiner, U., "Improved conductivity in dye-sensitised solar cells through block-copolymer confined TiO_2 crystallisation," *Energy & Environmental Science* **4**(1), 225–233 (2011).

[29] Docampo, P., Guldin, S., Stefik, M., Tiwana, P., Orilall, M. C., Hüttner, S., Sai, H., Wiesner, U., Steiner, U., and Snaith, H. J., "Control of solid-state dye-sensitized solar cell performance by block-copolymer-directed TiO_2 synthesis," *Advanced Functional Materials* **20**(11), 1787 – 1796 (2010).

[30] Snaith, H. J. and Schmidt-Mende, L., "Advances in liquid-electrolyte and solid-state dye-sensitized solar cells," *Advanced Materials* **19**(21), 3187–3200 (2007).